

A numerical model for transient simulation of porous wicked heat pipes by lattice Boltzmann method

Yonghua Huang*, Qiang Chen

Institute of Refrigeration and Cryogenics, Shanghai Jiao Tong University, Shanghai 200240, China



ARTICLE INFO

Article history:

Received 8 July 2016

Received in revised form 9 September 2016

Accepted 27 September 2016

Available online 13 October 2016

Keywords:

Heat pipe

Simulation

Transient

Lattice Boltzmann method

ABSTRACT

A numerical model based on an analytical lumped vapor assumption was proposed for highly efficient simulation of transient performances of heat pipes. The wick is modeled as fully thawed porous medium in which both the Darcian and non-Darcian effects are considered. The evaporation and condensation rates of the working substance are calculated locally as a function of not only the liquid–vapor interface temperature but also the vapor state properties by the kinetic theory. The coupled equations for liquid flow and heat conduction in/between components of the heat pipe are solved by a thermal lattice Boltzmann algorithm. Validation of the model is conducted by reproducing representative cases from the literature and then comparing the present results with their experimental and theoretical data. It turns out that both the transient temperature variation and the steady-state temperature and pressure profiles are in accordance with the literature results. The vapor velocity profile inferred from the evaporation rates is also found to be sufficiently accurate, which even gives a more reasonable estimate than the reference in comparison. In order to further improve the simulation efficiency of the code, non-uniform lattice and parallel algorithm are incorporated, based upon which the lumped vapor model achieves a speed over 50 times faster than the plain model with complete vapor consideration. The present model could serve as an efficient tool for quick evaluation of transient heat pipe behaviors and for assisting parametric studies of heat pipes.

© 2016 Elsevier Ltd. All rights reserved.

1. Introduction

Heat pipes transfer heat by using phase transition predominantly in addition to thermal conduction, which produces an equivalent conductivity of up to several orders of magnitude higher than that of pure metals. Theoretical modelings have been extensively implemented to study the operation performance of heat pipes due to the flexibility, convenience and low cost. Depending upon how the parts of heat pipe are modeled and solved, the modeling methods can be categorized as either analytical or numerical. Although these methods essentially solve the same heat transfer equations, the different perspectives taken in modeling the components result in different simulation efficiencies and different levels of understanding of the heat pipe mechanisms.

The analytical methods have been extensively studied for heat pipes. Despite the fact that the geometries of heat pipes are usually regular, the governing equations are almost impossible to be solved directly in an traditional analytical way due to the complex-

ity. Faghri and Harley [1] proposed a transient model for conventional as well as gas-loaded heat pipes. The components were modeled as lumped capacitances which greatly simplified the solution. Zhu and Vafai [2] developed an analytical model to study the startup characteristics of asymmetrical flat-plate and disk-shaped heat pipes. The liquid-saturated wick was treated as solid using a conduction model, and this wick model is then thermally coupled to a pseudo-3D vapor model. Zuo and Faghri [3] analyzed the transient temperature variation by considering the heat pipe as a network of components with conduction and convection. Similarly, Yadavalli *et al.* [4] used a 1-D thermal resistance network model to analyze the thermal performance thresholds of ultrathin flat heat pipes. Nouri-Borujerdi and Layegi [5] proposed a 1-D analytical model for the liquid flow in wick and compared with 2-D numerical results, and found that the analytical result is closer to the one predicted by the Darcy's law than the 2-D numerical model. Mistry *et al.* [6] adopted the growing thermal layer concept to solve the conduction in the wall and in the wick, and evaluated the transient and steady-state performances of the heat pipe. Although being computationally efficient in calculating simplified profiles of velocity, pressure and temperature, many analytical methods use only a few variables to describe the heat pipe, while

* Corresponding author.

E-mail address: huangyh@sjtu.edu.cn (Y. Huang).

Nomenclature

c_p	heat capacity	T	temperature
c_s	speed of sound	t	time
dx	lattice spacing in the X direction	T_{LV}	liquid-vapor interface temperature
dy	lattice spacing in the Y direction	T_V	vapor temperature
\mathbf{e}_i	discrete velocity set	T_{cool}	cooling water temperature
f_i	distribution function of flow field	T_∞	ambient radiation temperature
g_i	distribution function of temperature field	\mathbf{u}	velocity
h_{fg}	latent heat	X_a	position of adiabatic end
k_{eff}	effective thermal conductivity of wick	X_c	position of condensation end
k_{wall}	thermal conductivity of wall	X_e	position of evaporation end
M	molecular weight	α_m	effective thermal diffusivity
\dot{m}	evaporation rate	ϵ	porosity
m_V	mass of vapor	ν	viscosity
p	pressure	ν_e	effective viscosity
p_V	pressure in vapor core	ρ	density
p_{sat}	saturated vapor pressure	$\hat{\sigma}$	accommodation coefficient
R	universal gas constant	σ	heat capacity ratio between solid and fluid
R_x	aspect ratio of the lattice		

some rely on unrealistic assumptions like considering only thermal conduction in porous media. These factors restrict the applications of analytical methods in circumstances where thorough understanding of the flow and temperature fields is required.

Numerical methods, on the other hand, generally present a detailed view of each part of the heat pipe. The coupled conduction and convection equations are solved iteratively by discretizing the solid wall, wick, and vapor with control volumes or finite elements. The well-known general heat pipe solvers "HPTAM" [7] and "THROPUT" [8] are both based on this method. A major advantage of the numerical methods is the capability of calculating detailed temperature and flow fields, enabling much more flexible explorations on the performances of heat pipes. For instance, one can modify the numerical model by including more sophisticated governing equations to study the non-Darcian effects [9], or by conducting parametric investigations to learn the dry-out characteristics [10,11], effect of heating and cooling configurations [12], etc. The disadvantage of the numerical methods is its relatively higher expenses in computational cost and time consumption compared to the analytical methods, since usually a sufficiently large mesh is required to ensure reliable and accurate results. Although the numerical methods are useful for in-depth studies of heat pipes, it's less efficient for a large number of comparative cases, particularly for the transient simulations.

Transient performance is an important factor for evaluation of heat pipes. A number of transient studies on heat pipes focus on the startup process such as the low-temperature heat pipe starting from supercritical state or the high-temperature heat pipe starting from frozen state [13]. In those cases, the initiation of the phase change of the working fluid and thereafter the formation of the fluid circulation is the dominant phenomenon. In another scenario, the transient response to a heat load being suddenly applied or changed without a phase change from frozen or supercritical state is also of interest. For example, an abrupt increase of a CPU load could lead to a temperature rise of over 50 °C in a few seconds, and it is of great significance to see how quickly the heat pipe in the electric cooling device responds, and how long it takes to reach the steady working state.

This paper intends to present a numerical model for fast simulation of the transient behavior of heat pipes. The temperature and the pressure of the vapor region are treated as lumped parameters. Conduction in the wall and the wick, liquid flow in the wick, and phase change are numerically solved by the lattice Boltzmann

method (LBM). Our transient heat pipe model is fully capable of performing the above mentioned numerical methods for further analysis of the temperature and flow profiles. The inclusion of the lumped vapor consideration greatly lowers the total computational cost, which enables it to be an efficient tool for fast simulation of the transient processes of heat pipes.

2. Transient heat pipe model and numerical implementation

2.1. Physical and mathematical description of heat pipes

Conventionally, a heat pipe is divided into three thermally coupled parts: the solid wall (container), the wick filled with working fluid, and the vapor core. The working fluid undergoes continuous phase change between liquid and vapor, driven by the input heat and the capillary effect of the wick. The working mechanism of porous wicked heat pipes is schematically shown in Fig. 1.

Heat transfer in the wick includes conduction, convection and phase transition in saturated or unsaturated porous media. The wick is assumed to be fully thawed, in which the momentum equation for the working fluid follows the Brinkman-Forchheimer-ext ended Darcy model, including the linear (Darcy) term, the viscous (Brinkman) term and the non-linear (Forchheimer) term:

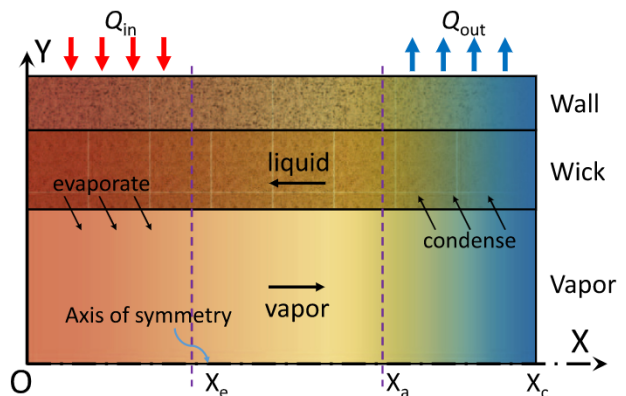


Fig. 1. Schematic of the working mechanism and boundary conditions of porous wicked heat pipes.

$$\frac{\partial \mathbf{u}}{\partial t} + (\mathbf{u} \cdot \nabla) \left(\frac{\mathbf{u}}{\epsilon} \right) = -\frac{1}{\rho} \nabla(\epsilon p) + v_e \nabla^2 \mathbf{u} + \mathbf{F} \quad (1)$$

where \mathbf{u} and p are the volume averaged velocity and pressure, respectively; t is the time; ϵ is the porosity; ρ is the density of the liquid; v_e is the effective viscosity. \mathbf{F} is the external force, including the one generated by the interaction between the porous media and the fluid (Darcy term and Forchheimer term):

$$\mathbf{F} = -\frac{\epsilon v}{K} \mathbf{u} - \frac{\epsilon F_\epsilon}{\sqrt{K}} |\mathbf{u}| \mathbf{u} + \epsilon \mathbf{G} \quad (2)$$

where K is the permeability; F_ϵ is the structural parameter of the porous media, and \mathbf{G} is the external force excluding the porous induced parts. The energy equation for the wick is:

$$\sigma \frac{\partial T}{\partial t} + \mathbf{u} \cdot \nabla T = \nabla \cdot (\alpha_m \nabla T) \quad (3)$$

where $\sigma = \epsilon + (1 - \epsilon) \rho_s c_{ps} / \rho_f c_{pf}$ is the ratio of the heat capacities between the solid and fluid phases; T is the temperature, and α_m is the effective thermal diffusivity.

Eqs. (1)–(3) also apply to the heat and mass transfer in the vapor core and in the heat pipe wall, since theoretically the solid and fluid could both be treated as special cases of porous media, with porosities equal to unity and zero for vapor and wall, respectively. Therefore, the governing equations for the three parts of heat pipes can actually be presented in the same form. As elaborated in the next section, a common set of lattice Boltzmann equations will be adopted to simulate the wall and porous wick. However, the vapor core will be treated as a lumped regime, for the sake of saving computational cost.

The boundary conditions of the heat pipe are handled as follows.

1. Heat input: Thermal load is applied on the outer wall of the evaporator section of the heat pipe, as in one of the following (based on the coordinates defined in Fig. 1):

- Fixed flux, $\partial T / \partial y = f(x), 0 < x < X_e$,
- Fixed temperature profile, $T = f(x), 0 < x < X_e$.

2. Heat rejection: The cooling conditions at the condenser section are in general one of the following ($X_a < x < X_c$):

- Fixed heat flux, $\partial T / \partial y = f(x)$,
- Fixed temperature, $T = f(x)$,
- Convective cooling, $\partial T / \partial y \propto (T - T_{cool})$,
- Radiative cooling, $\partial T / \partial y \propto (T^4 - T_\infty^4)$.

The first two items are extensively adopted as approximations to the actual condition. The convective cooling condition is mostly used in applications where the condenser section is cooled by water in the jacket. The radiative cooling condition could be applied to high temperature heat pipes used in satellites.

3. Wall-wick interface: The solid wall and the wick are thermally coupled without an internal heat source as $k_{wall} \times \partial T_{wall} / \partial y = k_{eff} \times \partial T_{wick} / \partial y$. The effective thermal conductivity of the wick k_{eff} is a combination of the contributions from the solid and the liquid. No-slip condition is applied to the flow field at this interface.

4. Liquid-vapor interface: The evaporation and condensation bring in mass transfer and latent heat transfer at both ends of the heat pipe. The evaporation rate can be specified in several ways, such as the one with kinetic method introduced in the following section. No-slip condition is also applied to the liquid, since the liquid flow near the interface is restricted by the capillary induced meniscus.

5. Symmetry plane: The center line of the vapor core can be treated as either mirror-symmetric or axial-symmetric axis. The former corresponds to planar vapor chambers and the latter corresponds to cylindrical heat pipes.

6. Other unspecified boundaries (eg. the end caps) of the heat pipes are adiabatic, i.e. $\partial T / \partial x = 0$.

Thermophysical properties of the working fluid, the wick and the wall can be considered either temperature-dependent or constant, depending on the temperature range of the actual application. The temperature-dependent option can be implemented by incorporating fitted equations or by loading third-party libraries, for instance the "REFPROP" [14] code from NIST. In the cases with insignificant temperature variation, properties such as the conductivity of the wall of heat pipes could be treated as constant, which still produce satisfying results.

2.2. Lumped vapor assumption and evaporation/condensation condition

Under most circumstances, the temperature gradient in the vapor core is relatively much smaller than those in the wick and the wall. Table 1 lists some experimental results from open literatures which compare the temperature differences in the wall and the vapor. Taking the experimental errors into consideration, it shows that the vapor part contributes very little to the total temperature difference across the heat pipe. This behavior is mostly due to the fact that the heat transfer in the vapor core is dominated by the diffusion of the vapor itself. The vapor flows quickly from the evaporator section to the condenser section, which helps suppress the growing of overall temperature difference in the vapor core. Such a uniform temperature behavior exists not only in the steady-state, but also in the transient process. It was found that the transient response of the vapor is much faster than the wick or the wall, making it almost always thermally quasi-equilibrium in transition processes [15,16].

Based on the uniformity behavior of the vapor observed in those cases, it is reasonable to have the vapor temperature represented by a lumped parameter assumption, which assumes the temperature of the vapor to be T_v throughout the whole vapor core. This assumption is valid for most heat pipes working under moderation conditions, except some unusual cases such as very high power input or very small vapor core size.

With the lumped vapor assumption, the enthalpy and mass of the vapor are then integrated with respect to time, from which the temperature T_v can be calculated. Converting this integration into iterative form, we get the following equations for the lumped vapor calculation:

$$m_v^{i+1} = m_v^i + \int_0^{X_c} \dot{m} dx \quad (4)$$

$$T_v^{i+1} = \frac{T_v \times m_v^i + \int_0^{X_c} \dot{m} \cdot T_{LV}(x) dx}{m_v^{i+1}} \quad (5)$$

where the superscripts i and $i + 1$ are the iteration indices; \dot{m} is the evaporation rate, and T_{LV} is the temperature at the liquid-vapor interface.

The evaporation/condensation condition is applied through the equation based on the kinetic theory that relates the

Table 1
Experimental temperature difference in wall and vapor in literature.

Reference	ΔT_{wall}	ΔT_{vapor}
Gernert [17]	~ 9 K	< 1 K
El-Genk & Huang [18]	~ 25 K	~ 1 K
Schmalhofer & Faghri [19]	~ 13 K	~ 2 K
	~ 40 K	~ 2 K
Huang et al. [20]	~ 28 K	< 1 K

evaporation/condensation rate to the liquid–vapor interface temperature and the state properties of the vapor:

$$\dot{m} = \frac{2\hat{\sigma}}{2 - \hat{\sigma}} \left(\frac{M}{2\pi\bar{R}} \right)^{0.5} \left(\frac{p_{\text{sat}}(T_{\text{LV}})}{T_{\text{LV}}^{0.5}} - \frac{p_{\text{V}}}{T_{\text{V}}^{0.5}} \right) \quad (6)$$

where $\hat{\sigma}$ is the accommodation coefficient, M is the molecular weight of the working substance, and \bar{R} is the universal gas constant. The pressure of the vapor, p_{V} , is approximately equal to the saturated pressure corresponding to T_{V} , $p_{\text{sat}}(T_{\text{V}})$. Here, the subscript “sat” is the abbreviation of “saturation”.

The greatest contribution of introducing the lumped vapor assumption is that the numerical solution in this regime is omitted. Since the radius of the vapor core in most cases is at least over 5 times larger than the thickness of the wick and wall, this lumped vapor assumption would save a significant portion of the total computational cost. The details on the numerical performance of the model will be benchmarked and compared in Section 3.4. Despite the simplicity of the lumped vapor consideration, the lumped vapor heat pipe model (LVHPM) still produces fairly accurate results, as shown by the verification cases in Sections 3.1 and 3.2.

2.3. Numerical method and its implementation

Lattice Boltzmann is a numerical method based on the Boltzmann transport equation with a wide range of applications [21–23]. In order to simulate the transient process of heat pipes, the lattice Boltzmann method is a more suitable choice compared to other conventional CFD methods. Firstly, LBM uses relaxation method to explicitly simulate the time-march processes. Such an intrinsic dynamic characteristic makes it a good tool for studying problems that focus on time-dependent effects. Secondly, most heat pipes have ideally regular geometry, which could be easily meshed with uniform grid as required by the standard LBM. It also means that simulating heat pipes with different geometry requires very little change in the code. There is no need to go through the re-meshing and re-configuring processes which are normally required by commercial CFD packages like FLUENT.

To solve the process integrated with thermally coupled conduction, liquid flow, liquid evaporation and vapor condensation, the generalized lattice Boltzmann equation (LBE) coupled with thermal LBE proposed by Guo and Zhao [24] is adopted. The generalized LBE model is suitable for this application because its equivalent macroscopic form, as shown in Eqs. (1)–(3), is simultaneously applicable to the wall, the vapor and the liquid in porous media. The wick simulation uses the full equations, while the simulation of the solid wall uses the equations with constant density and zero velocity. The vapor simulation is not required here, due to the assumption made in Section 2.2, although it could use the same equations with the porosity set to 1.

The flow in porous media is given by the evolution of distribution functions f_i ,

$$f_i(\mathbf{x} + \mathbf{e}_i \delta t, t + \delta t) = f_i(\mathbf{x}, t) + \frac{1}{\tau} [f_i(\mathbf{x}, t) - f_i^{\text{eq}}(\mathbf{x}, t)] + \delta t F_i \quad (7)$$

where \mathbf{x} and t are the position and time, respectively; \mathbf{e}_i is the discrete velocity set; δt is the time step for each iteration; τ is the relaxation time. The equilibrium distribution function f_i^{eq} for the D2Q9 (2-dimension, 9 discrete velocities) model used in this work is defined as,

$$f_i^{\text{eq}} = \omega_i \rho \left[1 + 3 \cdot \mathbf{e}_i \cdot \mathbf{u} + 4.5 \cdot \frac{\mathbf{u}\mathbf{u} : (\mathbf{e}_i \mathbf{e}_i - \frac{1}{3} \mathbf{I})}{2\epsilon} \right] \quad (8)$$

where ω_i is the weight for each direction of the discrete velocities and \mathbf{I} is the identity matrix.

The external force term is given by,

$$F_i = \omega_i \rho \left(1 - \frac{1}{2\tau} \right) \left[3 \cdot \mathbf{e}_i \cdot \mathbf{F} + 9 \cdot \frac{\mathbf{u}\mathbf{F} : (\mathbf{e}_i \mathbf{e}_i - \frac{1}{3} \mathbf{I})}{\epsilon} \right] \quad (9)$$

Accordingly, the fluid density ρ and velocity \mathbf{u} can be written as,

$$\rho = \sum_i f_i \quad (10)$$

$$\mathbf{u} = \frac{\mathbf{v}}{c_0 + \sqrt{c_0^2 + c_1 |\mathbf{v}|}}, \text{ where } \mathbf{v} = \left(\sum_i \mathbf{e}_i f_i + \frac{1}{2} \epsilon \rho \mathbf{G} \right) / \rho \quad (11)$$

The coefficients in Eq. (11) are given by $c_0 = 0.5(1 + 0.5\epsilon v/K)$, $c_1 = 0.5\epsilon F_\epsilon / \sqrt{K}$ ($F_\epsilon = 1.75/\sqrt{150\epsilon^3}$).

In addition to the flow field, another set of distribution functions is needed to simulate the temperature field. The evolution equation and the equilibrium temperature distribution are written as Eqs. (12) and (13), respectively.

$$g_i(\mathbf{x} + \mathbf{e}_i \delta t, t + \delta t) = g_i(\mathbf{x}, t) + \frac{1}{\tau} [g_i(\mathbf{x}, t) - g_i^{\text{eq}}(\mathbf{x}, t)] \quad (12)$$

$$g_i^{\text{eq}} = \omega_i T (1 + 3 \mathbf{e}_i \cdot \mathbf{u}) \quad (13)$$

where the temperature is given by,

$$T = \frac{1}{\sigma} \sum_i g_i \quad (14)$$

The boundary conditions for no-slip, heat flux or constant temperature are all implemented by the non-equilibrium extrapolation method [25]. Evaporation and condensation are applied as energy source and mass sources, calculated by the evaporation Eq. (6).

3. Model verification and discussions

3.1. Simulation of transient processes

The transient simulation capability of the present model is validated by reproducing two cases from literature. These two cases are based on experimental results by Huang *et al.* [20] and Mistry *et al.* [6], whose boundary conditions are consistent with those shown in Fig. 1. Setup information of the two cases are listed in Table 2. Before running the simulations, meshing independence of both cases had been checked for the temperature, velocity and pressure. The mesh number chosen finally are 4.5×10^4 and 2.0×10^4 , respectively.

Fig. 2 compares the numerical result by the present study with (1) measured vapor temperature [20], and (2) numerical results by the same group [26]. With a total length of 89 cm and diameter of 19.1 mm, case (I) is a typical representative of long cylindrical heat pipes supplied with a large heat flux (443 W). As shown in the

Table 2
Working condition and boundary setup of cases for verification.

	Case (I) Huang <i>et al.</i> [20]	Case (II) Mistry <i>et al.</i> [6]
Working fluid	Water	Water
Wick type	Copper screen	SS-304 screen
Wick configuration	150 mesh, 2 layers	80 mesh, 6 layers
Wick thickness	0.75 (mm)	1.72 (mm)
Wick porosity	0.9	0.6305
Wick permeability	$1.5 \times 10^{-9} \text{ m}^2$	$3 \times 10^{-10} \text{ m}^2$
Lengths of sections	60/9/20 (cm)	8.467/11.85/5.08 (cm)
Outer diameter	19.1 (mm)	9.5 (mm)
Heat input	443 (W)	8.346/9.74/12.53 (W)
Cooling condition	Water cooling, 11.33 g/s	Water cooling (unknown)

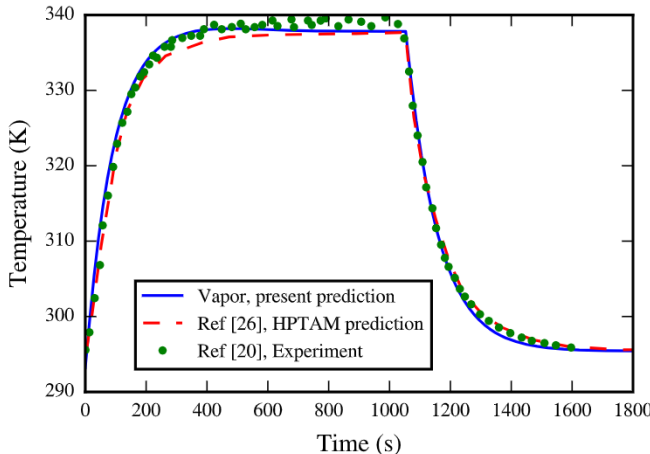


Fig. 2. Comparison of the vapor temperature curve for heat pipe startup and cool down processes between the present prediction and the literature results [20,26].

figure, the present model gives a good overall prediction on the transitional performance of the complete process. In the startup stage after heat is suddenly loaded, the prediction by the present model is slightly higher than the contrasting results in literature. Later in the process, the deviation from the experimental result decreases, and the present model produces a better curve than the HPTAM. For the cool down process, the present model responds slightly faster than the referred experiments and numerical results, but within a maximum temperature deviation of 3 K. For the sake of more revealing in regions of fast temperature change, the derivative of dT/dt is also presented as Fig. 3. It clearly shows that the derivative curves predicted by HPTAM and the present model are almost identical. Although the experimental data scattered due to their uncertainty, they agree well with the theoretical predictions in the trend.

For case (II), the present numerical result is validated through comparison with measurements by Mistry *et al.* [6], as well as their 1D and 2D theoretical modeling results. Fig. 4 provides simulations for two cases with different input power. This case represents a class of middle-length heat pipes supplied with low heat flux. It can be clearly seen that the results for both conditions are quite similar, in which the present result agrees better with the 2D model than the 1D model, the latter deviating largely from the measurements. In the early stage of the startup process, the present model predicts higher temperatures than the 2D model. The

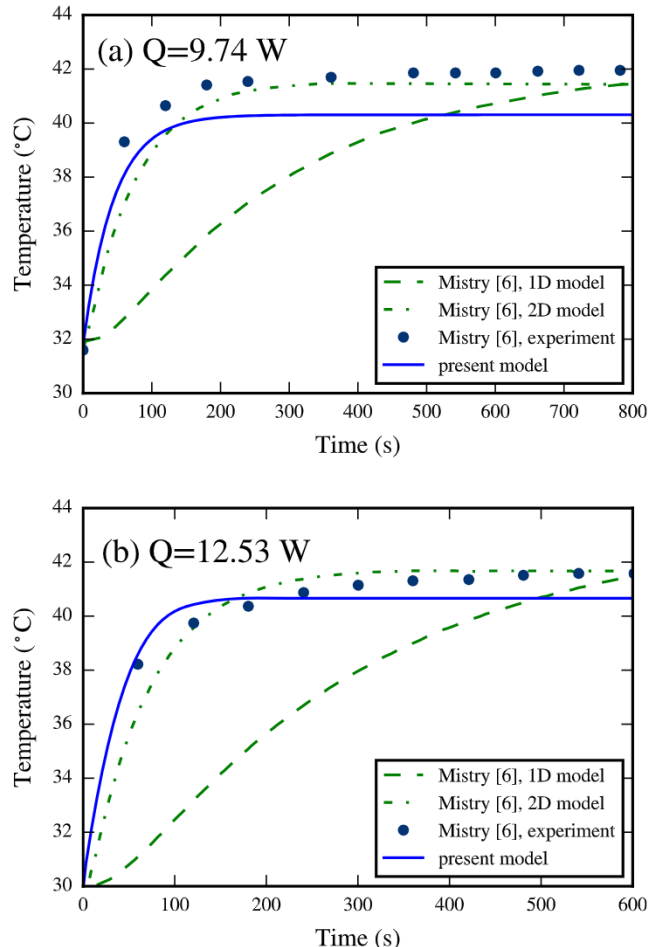


Fig. 4. Comparison of adiabatic wall temperature in the startup process between predictions by present model and literature results [6].

predicted curves also reach steady-states faster than the 2D model, which is more compliant with the measured transient temperature behavior. On the other hand, the present model slightly underestimates the steady temperature for less than 2 K in both conditions. The reason may be partly due to that the adiabatic temperature curve by the present model is extracted at the midpoint of the wall of the adiabatic section, whereas in the original reference the exact position of the measurement was not explicitly stated.

Both of these transient simulation cases indicate that the present lumped vapor heat pipe model is suitable for simulating the transient temperature behavior of heat pipes, although it slightly deviates from the more sophisticated models in the test cases. Overall, the LVHPM is capable of making good estimates of the temporal temperature variation for different geometries and heat loads.

3.2. Simulation of steady-state processes

As illustrated by Figs. 2 and 4, the heat pipe reaches steady state as time goes on, during which the temperature variation caused by the change of external heat load gradually diminishes. In the steady-state, the thermal performance of heat pipes is of great interest in terms of the operation temperature and the effective thermal conductivity. In this part, the steady-state performances of the above heat pipe cases are evaluated.

For Case (I) in Table 2, the vapor temperature and wall temperature along the length at steady-state are calculated and plotted in

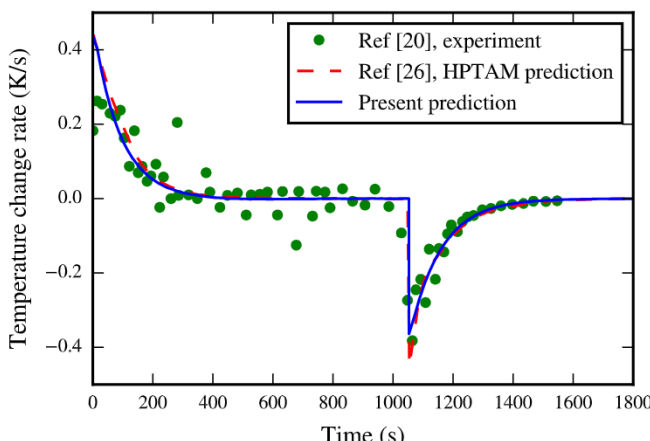


Fig. 3. Comparison of the temperature change rate between the present prediction and the literature results [20,26].

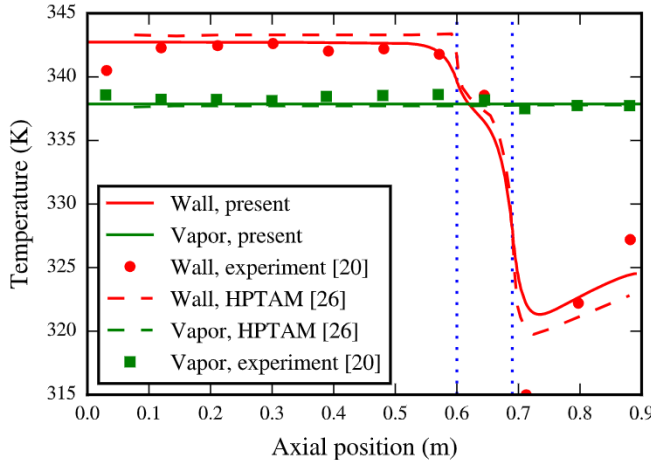


Fig. 5. Comparison of steady-state temperature profiles in vapor and wall between present model and Ref. [20,26].

Fig. 5. The vapor temperature predicted by the LVHPM agrees well with the experimental results by Huang *et al.* [20]. The lumped vapor assumption assumes uniform temperature throughout the vapor core therefore it could not predict the small temperature difference (~ 1 K) along the length as shown in the measurements. However, the average vapor temperature value predicted by the present model agrees with the measurements within a deviation of less than 1 K. The predicted wall temperature in the evaporator section agrees with the experimental data better than the values by the HPTAM. In the condenser section, the measurements considerably deviate from both the HPTAM modeling curve and the present modeling curve, although they have close mean values. The reason is thought to be that the temperature sensors installed in the condensation section were exposed to the cooling water and the wall temperature measurements were lowered by the coolant flow, especially at the inlet.

The wall temperature curves of Case (II) are shown in **Fig. 6**, also with two input power conditions of 9.74 and 8.346 W, respectively. Generally, the theoretically predicted curves have similar curvatures throughout the whole length of the heat pipes. The overall temperature difference predicted by the present model is closer to the experimental values than their analytical model. It indicates that the LVHPM is more accurate in predicting the effective thermal conductivity of the heat pipe based upon the overall temperature difference. It is also interesting to find that the LVHPM model does not produce the remarkable stair-shaped temperature feature of the heat pipe wall as did by the analytical model, especially in the adiabatic section. The stair-shaped temperature profile is usually observed in heat pipes with higher heat inputs, which is due to more phase change heat transfer than solid conduction, like the one shown in **Fig. 5**. However, the cases shown in **Fig. 6** have rather low heat inputs. The discrepancy could be due to underestimation of the axial conduction in the thermal layer model used in the reference. The abrupt temperature drop at the front of the condensation section in the experiment is considered to be due to the influence by the inflow of the cooling water as mentioned before. However, since data of the mass flux or the temperature of the cooling water is not available from the reference, it is not possible to have the exact condition for the condensation section in the present simulation. The approximation of the cooling boundary condition is thought to be the key reason for the deviation at $x > 0.7$.

These cases for comparison on heat pipes with various lengths and heat inputs show that the LVHPM is also adequate for predicting the steady-state temperature behavior. With this ability, the LVHPM can be used to analyze or optimize the thermal

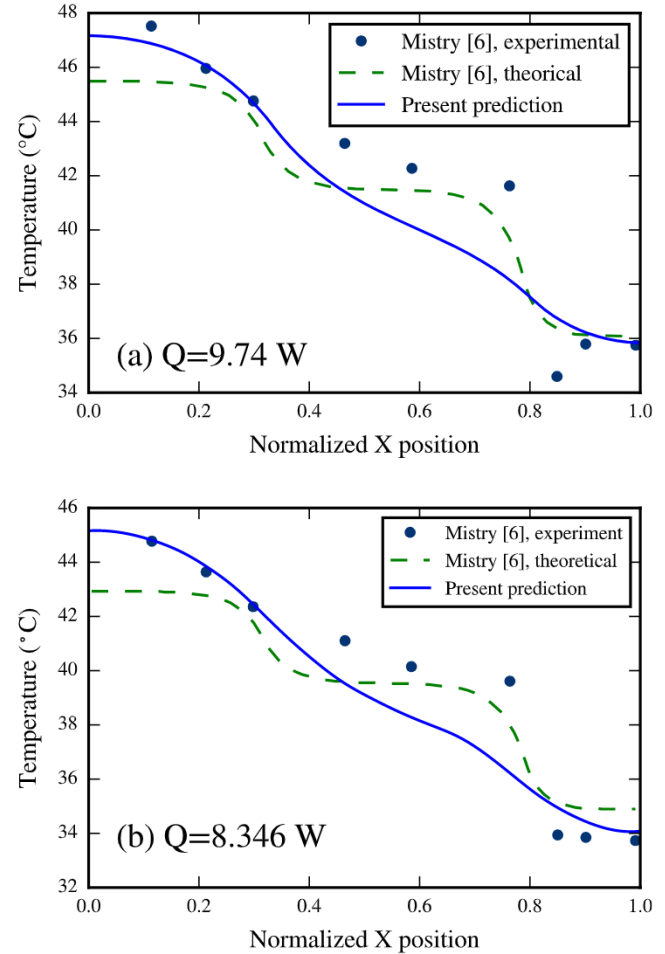


Fig. 6. Steady-state wall temperature profile by present model and Ref. [6].

performance of heat pipes via parametric studies, which means it could serve as a practical tool for heat pipe design.

3.3. Pressure and velocity behavior of working fluid

The above subsections focus on the temperature profiles as the primary measure of the thermal performances of heat pipes. However, the pressure and velocity characteristics are also of great interest due to the fact that they are closely related to some critical performances, for instance the capillary limit and the sonic limit.

The pressure field in the wick can be directly exported from the lattice Boltzmann simulation result, given by $p(x, y) = c_s^2 \rho(x, y)/\epsilon$. It should be pointed out that the pressure in the vapor part is actually approximated as the saturated vapor pressure corresponding to the vapor temperature, $p_v = p_{\text{sat}}(T_v)$, which has already been declared in the introduction of the lumped assumption. The steady-state pressure profile for Case (I) in **Table 2** is given in **Fig. 7**. The vapor and liquid pressure calculated by the present model are compared with the numerical results from Ref. [26] and the analytical result from Ref. [9] as shown in **Fig. 7**. It can be seen that the LVHPM accurately predicted the vapor pressure, even though it only uses a single pressure value. The liquid pressure curve fits both the analytical and numerical results in a considerably good agreement.

The velocity field of the liquid in the wick could also be directly extracted by Eq. (11) from the simulation. Meanwhile, the vapor velocity could be derived indirectly from the evaporation rate distribution. For a given position $X(x)$ in the vapor core, the mass flux

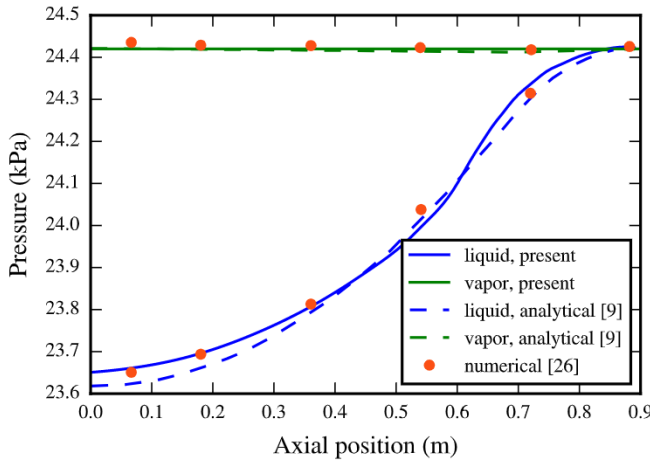


Fig. 7. Comparison of the pressure profiles predicted by the current model with literature results.

through a cross-sectional plane can be calculated by integrating the evaporation or condensation rate from the evaporation end to that position. Then the mean velocity at position X is calculated as follows,

$$u_V = m_V(X) / \left(\rho_V \times \frac{1}{4} \pi D_V^2 \right), \quad m_V(X) = \int_0^X \dot{m} \times \pi D_V \times dx \quad (15)$$

where D_V is the diameter of the vapor core.

The velocity profile for Case (I) calculated from Eq. (15) is shown in Fig. 8, in which the mean vapor velocity profile predicted by the current model appears beneath the analytical one by Zhu and Vafai [9]. However, there is a theoretical maximum mean vapor velocity ($Q_{in}/(h_{fg}\rho_V \times \frac{1}{4} \pi D_V^2)$) that occurs only when all the heat input is transferred through phase change of the working fluid. The theoretical maximum mean velocity is calculated and plotted as the horizontal dashed line in the same figure. It shows that the analytical curve is above this limit in the adiabatic section, while the LVHPM curve is close but kept strictly below that. In addition, the analytical vapor velocity profile shows that the velocity at the adiabatic section is constant, which essentially means absolute exclusion of evaporation and condensation. This result is contradictory to the practical fact that the liquid–vapor interface at the adiabatic section is actually not “adiabatic”. The evaporation

rate in this section continually transits from positive to negative instead of being a constant. The velocity magnitude reaches the maximum when the evaporation rate turns to zero.

The centerline velocity can also be inferred by taking the laminar flow assumption. Since the cross-sectional velocity profile is parabolic, the centerline velocity is simply double the mean velocity. Similar to the mean velocity as shown in Fig. 8, the laminar flow inferred velocity at the centerline is also significantly lower than that of the numerical and analytical results. Based upon these analysis, it is believed that the present curve is a more accurate estimate.

3.4. Solver performance improvements

The lumped vapor assumption used in the present model avoids direct simulation of the vapor part. Compared to the models with complete vapor considerations, the present LVHPM only solves the accumulative mass and energy equations given by Eqs. (4) and (5). In practice, the accumulation algorithm can be processed together with the liquid–vapor interface boundary, which incurs very little computational cost. Using the same case from Ref. [20] as an example, the thicknesses of the vapor core is around 8 times larger than that of the wick or the wall. It means that the required number of mesh for the vapor part is averagely over 4 times of that of the combined number in the wick and the wall, even with local densification method. In other words, for this case the lumped vapor model uses only 20% of the computational cost required by the complete vapor model.

In addition, the algorithm of non-uniform mesh [27] is incorporated in the present work to overcome the large aspect-ratio problem. In standard lattice Boltzmann model, mesh in the form of regular grid with equal spacing in X and Y directions is required so that the pseudo particles travel to the exact grid point nearby after each propagation step. For non-uniform mesh, in particular for grid with unequal gaps in X and Y directions, He *et al.* [27] proposed that an interpolation step should be added after the propagation in order to obtain the correct density distribution functions. In the present model, we used quadratic Lagrange interpolation, and extended this idea to the temperature distribution functions as well. In order to further reduce the computational load, the propagation and interpolation steps were combined into one step. Using the dimensionless units $\delta y = 1$, and $R_x = \delta x/\delta y$, the distribution function of any point (x,y) can be calculated as follows,

$$f_i(x, y, t+1) = \frac{R_x + 1}{2R_x^2} \times f_i(x - R_x e_{i,0}, y, t) + \frac{R_x^2 - 1}{R_x^2} \times f_i(x, y, t) + \frac{1 - R_x}{2R_x^2} \times f_i(x + R_x e_{i,0}, y, t) \quad (16)$$

The non-uniform LBM brings in a small additional computation cost for each iteration (less than 20% in the present code). However, given that the grid size for aspect ratio of R_x is only $1/R_x$ of the uniform counterpart, and that the interpolation is accurate for R_x up to 8 [27], the non-uniform algorithm is a significant boost for the simulation.

Lastly, parallelism based on OpenMP is adopted in the present code for the sake of the advantage of the parallel nature of the lattice Boltzmann method. A vertical column of grid nodes are used as the basic solution unit, then the solution units are dynamically dispatched to the threads running in parallel. This is similar to the partitioning method used by many conventional CFD solvers but with higher flexibility. The parallelism enables full usage of the large scale parallel processors offered by supercomputers. The present parallel LBM computation code has been successfully applied

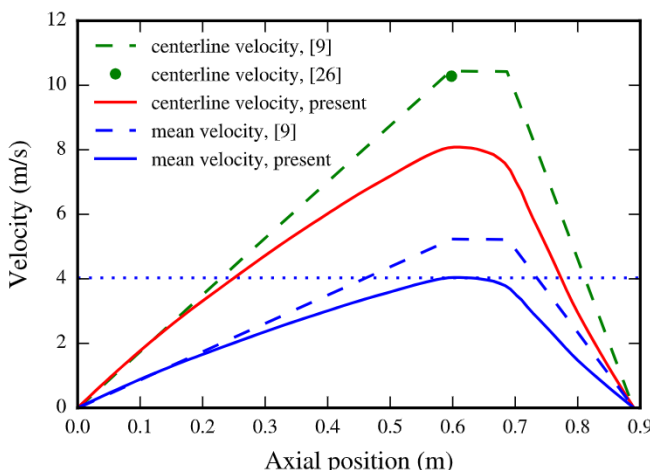


Fig. 8. Comparison of the vapor velocity profile predicted by the current model with literature results.

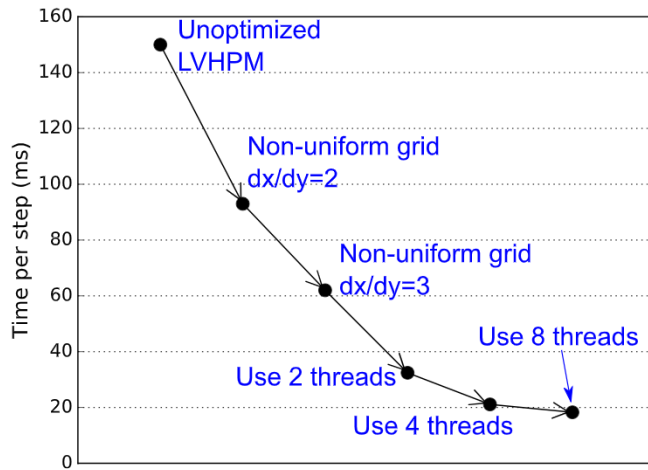


Fig. 9. Performance gains by using lumped vapor model, non-uniform mesh and parallelism (All benchmarks are run on an Intel 4770 K CPU. Grid number is 13×10^4 for the unoptimized LVHMP).

in the National Supercomputing Center at Shenzhen with Intel architectures.

A comparison of the performance benchmarks is shown in Fig. 9, using the same case setup from Ref. [20]. After adopting non-uniform algorithm and parallelism, the time required for a standard testing simulation reduces about 88% of that of the unoptimized LVHMP.

Combining the theoretical simplifications by the lumped vapor assumption and optimization techniques for LBM, the optimized heat pipe model is significantly more efficient than those adopting the complete vapor model. Since the unoptimized model with lumped vapor assumption is already at least 6 times faster than the complete vapor model, the optimized LVHMP runs approximately 50 times faster totally by a conservative estimate.

3.5. Applicability and limitations of current version model

The verification cases with input power up to over 400 W and total length from 25 to 89 cm (aspect ratio of 26.7 to 46.6) have shown that the assumption is applicable in a wide range of conditions. It indicates that the model is applicable to most moderate practical heat pipes which lie in the ranges of the above geometries and power inputs. For cases beyond the specific conditions evaluated, the applicability can be tested by estimating ΔT_v (temperature difference in the vapor core), or more precisely ΔT_{LV} (temperature difference throughout the liquid/wick-vapor interface). The liquid/wick-vapor (LV) temperature profile is normally very close to that of the vapor, because a small difference between them is sufficient to cause a very large evaporative heat flux, which basically means that $\Delta T_{LV} \approx \Delta T_v$. It was found that the lumped vapor assumption is appropriate when $\Delta T_{LV}/\Delta T_s \leq 0.1$ based on the following consideration: The simulation of the wick and the wall depends on the external wall surface and the liquid-vapor interface. Generally, the temperature difference between the two ends on the former (ΔT_s) is about one order of magnitude higher than that on the latter (ΔT_{LV}), for example in the case (I), being ~ 21 K and ~ 1 K, respectively. Therefore, Ignoring ΔT_{LV} at the liquid-vapor interface will not affect the wick simulation when $\Delta T_{LV} \ll \Delta T_s$. The estimation of ΔT_{LV} could be achieved by adopting the thermal network model by Zuo and Faghri [3]. Generally, estimating ΔT_{LV} is required only once for parametric studies with batch of transient simulations. This additional time cost is acceptable compared to the total time.

Further, a limitation of the current model is that the current implementation has a relatively lower efficiency in simulating the steady-state cases. The standard LBM with LBGK approximation is an explicit time-marching method. To obtain steady results, it requires initialization at a forecast state near equilibrium, and a development process before steady-state. However, the “forecast” work is manual and cannot be done by the solver automatically. In the future, efforts on developing methods to accelerate the steady-state simulations will be made, for example, by referring to the better pre-conditioning methods [28,29], using local time step [30], or modifying and integrating other efficient steady-state method [31], etc.

4. Conclusions

A numerical model LVHMP for simulating the transient processes of heat pipes is presented. It uses lumped assumption for the vapor core, using a single saturated state property to describe the whole vapor. By this assumption, the physical model and governing equations are significantly simplified. The LVHMP, implemented with lattice Boltzmann method, requires much less computational resources due to the proposed treatment, while it also retains the ability of detailed analysis on the processes of the conduction, fluid flow in wick, evaporation and condensation. Verification of the model is conducted by using it to reproduce cases from literature, from which it is demonstrated that the model is capable of accurately simulating the transient process of heat pipes as well as the steady-state behaviors. Some of the predictions were found to slightly deviate from the reference values, for which reasonable explanations were presented. To achieve optimized efficiency, non-uniform grid and parallel algorithm are adopted. Compared to the complete vapor model, the present model works around 50 times faster for transient simulations in the test.

Acknowledgement

We gratefully acknowledge the financial support from the National Natural Science Foundation of China (No. 51176112).

References

- [1] A. Faghri, C. Harley, Transient lumped heat pipe analyses, *Heat Recovery Syst. CHP* 14 (4) (1994) 351–363, [http://dx.doi.org/10.1016/0890-4332\(94\)90039-6](http://dx.doi.org/10.1016/0890-4332(94)90039-6).
- [2] N. Zhu, K. Vafai, Analytical modeling of the startup characteristics of asymmetrical flat-plate and diskshaped heat pipes, *Int. J. Heat Mass Transfer* 41 (17) (1998) 2619–2637, [http://dx.doi.org/10.1016/S0017-9310\(97\)00325-6](http://dx.doi.org/10.1016/S0017-9310(97)00325-6).
- [3] Z. Zuo, A. Faghri, A network thermodynamic analysis of the heat pipe, *Int. J. Heat Mass Transfer* 41 (11) (1998) 1473–1484, [http://dx.doi.org/10.1016/S0017-9310\(97\)00220-2](http://dx.doi.org/10.1016/S0017-9310(97)00220-2).
- [4] Y. Yadavalli, J.A. Weibel, S.V. Garimella, Flat heat pipe performance thresholds at ultra-thin form factors, in: *Therm. Thermomech. Phenom. Electron. Syst. (ITHERM)*, IEEE, 2014, pp. 527–534, doi: <http://dx.doi.org/10.1109/ITHERM.2014.6892326>.
- [5] A. Nouri-Borjerdi, M. Layeghi, Liquid flow analysis in concentric annular heat pipes wicks, *J. Porous Media* 8 (5) (2005) 471–480.
- [6] P.R. Mistry, F.M. Thakkar, S. De, S. DasGupta, Experimental validation of a two-dimensional model of the transient and steady-state characteristics of a wicked heat pipe, *Exp. Heat Transfer* 23 (4) (2010) 333–348, <http://dx.doi.org/10.1080/08916150903564804>.
- [7] J.-M. Tournier, M.S. El-Genk, HPTAM for modeling heat and mass transfers in a heat pipe wick, during startup from a frozen state, *Proceedings of the 12th Symposium on Space Nuclear Power and Propulsion: Conference on Alternative Power from Space; Conference on Accelerator Driven Transmutation Technologies and Applications*, vol. 32, AIP, 1995, pp. 123–134, doi: <http://dx.doi.org/10.1063/1.47213>.
- [8] M.L. Hall, Status report on the THROPUT transient heat pipe modeling code, in: *Proceedings of the Eleventh Symposium on Space Nuclear Power and Propulsion, Albuquerque*, 1994, pp. 965–970.
- [9] N. Zhu, K. Vafai, Analysis of cylindrical heat pipes incorporating the effects of liquid-vapor coupling and non-Darcian transport – a closed form solution, *Int. J. Heat Mass Transfer* 42 (18) (1999) 3405–3418, [http://dx.doi.org/10.1016/S0017-9310\(99\)00017-4](http://dx.doi.org/10.1016/S0017-9310(99)00017-4).

- [10] B. Suman, S. De, S. DasGupta, A model of the capillary limit of a micro heat pipe and prediction of the dry-out length, *Int. J. Heat Fluid Flow* 26 (3) (2005) 495–505, <http://dx.doi.org/10.1016/j.ijheatfluidflow.2004.09.006>.
- [11] J.A. Rice, A. Faghri, Analysis of screen wick heat pipes, including capillary dry-out limitations, *J. Thermophys. Heat Transfer* 21 (3) (2007) 475–486, <http://dx.doi.org/10.2514/1.24809>.
- [12] M. Aghvami, A. Faghri, Analysis of flat heat pipes with various heating and cooling configurations, *Appl. Therm. Eng.* 31 (14–15) (2011) 2645–2655, <http://dx.doi.org/10.1016/j.applthermeng.2011.04.034>.
- [13] M. El-Genk, J.-M. Tournier, Challenges and fundamentals of modeling heat pipes startup from a frozen state, *Space Technology and Applications International Forum- STAIF 2002*, Albuquerque, New Mexico (USA), vol. 608, 2002, pp. 127–138, doi: <http://dx.doi.org/10.1063/1.1449717>.
- [14] E.W. Lemmon, M.L. Huber, M.O. McLinden, NIST reference fluid thermodynamic and transport properties-REFPROP, Version 9.1 Colorado: National Institute of Standard Technology, Version, 2013.
- [15] W.S. Chang, G.T. Colwell, Mathematical modeling of the transient operating characteristics of a low-temperature heat pipe, *Numer. Heat Transfer* 8 (2) (1985) 169–186, <http://dx.doi.org/10.1080/01495728508961848>.
- [16] W.J. Bowman, J. Hitchcock, A compressible vapor flux model for transient heat pipe analysis, in: *Transactions of the 4th Symposium on Space Nuclear Power Systems*, 1987, pp. 358–388, Albuquerque, New Mexico (USA).
- [17] N. Gernert, Analysis and performance evaluation of heat pipes with multiple heat sources, *4th Joint Thermophysics and Heat Transfer Conference*, vol. 1, 1986.
- [18] M.S. El-Genk, L. Huang, An experimental investigation of the transient response of a water heat pipe, *Int. J. Heat Mass Transfer* 36 (15) (1993) 3823–3830, [http://dx.doi.org/10.1016/0017-9310\(93\)90062-B](http://dx.doi.org/10.1016/0017-9310(93)90062-B).
- [19] J. Schmalhofer, A. Faghri, A study of circumferentially-heated and block-heated heat pipes-I. Experimental analysis and generalized analytical prediction of capillary limits, *Int. J. Heat Mass Transfer* 36 (1) (1993) 201–212, [http://dx.doi.org/10.1016/0017-9310\(93\)80080-E](http://dx.doi.org/10.1016/0017-9310(93)80080-E).
- [20] L. Huang, M.S. El-Genk, J.-M. Tournier, Transient performance of an inclined water heat pipe with a screen wick, in: *ASME National Heat Transfer Conference*, vol. 236, Atlanta, GA, USA, 1993, pp. 87–92.
- [21] M. Sheikholeslami, M. Gorji-Bandpy, K. Vajravelu, Lattice boltzmann simulation of magnetohydrodynamic natural convection heat transfer of al2o3water nanofluid in a horizontal cylindrical enclosure with an inner triangular cylinder 80 16–25. doi: <http://dx.doi.org/10.1016/j.ijheatmasstransfer.2014.08.090>.
- [22] M. Sheikholeslami, R. Ellahi, Three dimensional mesoscopic simulation of magnetic field effect on natural convection of nanofluid 89 799–808. doi: <http://dx.doi.org/10.1016/j.ijheatmasstransfer.2015.05.110>.
- [23] Y. Huang, Q. Chen, Numerical investigation on thermal effects by adding thin compartmental plates into cooling enclosures with heat-leaking walls 17 (6) 485–496. doi: <http://dx.doi.org/10.1631/jzus.A1500319>.
- [24] Z. Guo, T.S. Zhao, A lattice Boltzmann model for convection heat transfer in porous media, *Numer. Heat Transfer, Part B: Fundam.* 47 (2) (2005) 157–177, <http://dx.doi.org/10.1080/10407790590883405>.
- [25] Z. Guo, C. Zheng, B. Shi, An extrapolation method for boundary conditions in lattice Boltzmann method, *Phys. Fluids* 14 (6) (2002) 2007–2010, <http://dx.doi.org/10.1063/1.1471914>.
- [26] J.-M. Tournier, M. El-Genk, A heat pipe transient analysis model, *Int. J. Heat Mass Transfer* 37 (5) (1994) 753–762, [http://dx.doi.org/10.1016/0017-9310\(94\)90113-9](http://dx.doi.org/10.1016/0017-9310(94)90113-9).
- [27] X. He, L.-S. Luo, M. Dembo, Some progress in lattice Boltzmann method. Part I. Nonuniform mesh grids, *J. Comput. Phys.* 129 (2) (1996) 357–363, <http://dx.doi.org/10.1006/jcph.1996.0255>.
- [28] Z. Guo, T. Zhao, Y. Shi, Preconditioned lattice-Boltzmann method for steady flows, *Phys. Rev. E* 70 (6) (2004) 066706, <http://dx.doi.org/10.1103/PhysRevE.70.066706>.
- [29] S. Izquierdo, N. Fueyo, Optimal preconditioning of lattice Boltzmann methods, *J. Comput. Phys.* 228 (17) (2009) 6479–6495, <http://dx.doi.org/10.1016/j.jcp.2009.05.040>.
- [30] T. Imamura, K. Suzuki, T. Nakamura, M. Yoshida, Acceleration of steady-state lattice Boltzmann simulations on non-uniform mesh using local time step method, *J. Comput. Phys.* 202 (2) (2005) 645–663, <http://dx.doi.org/10.1016/j.jcp.2004.08.001>.
- [31] J. Wu, P. Huang, X. Feng, D. Liu, An efficient two-step algorithm for steady-state natural convection problem 101, 387–398. doi: <http://dx.doi.org/10.1016/j.ijheatmasstransfer.2016.05.061>.